7992–8004 *Nucleic Acids Research, 2011, Vol. 39, No. 18* *Published online 6 July 2011*
doi:10.1093/nar/gkr280

XRCC1 haploinsufficiency in mice has little effect on aging, but adversely modifies exposure-dependent susceptibility

Daniel R. McNeill[1], Ping-Chang Lin[2], Marshall G. Miller[3], Paul J. Pistell[4], Nadja C. de Souza-Pinto[5], Kenneth W. Fishbein[2], Richard G. Spencer[2], Yie Liu[1], Christina Pettan-Brewer[6], Warren C. Ladiges[6,*] and David M. Wilson III[1,*]

[1]Laboratory of Molecular Gerontology, [2]Laboratory of Clinical Investigation, National Institute on Aging, National Institutes of Health, IRP, Biomedical Research Center, Baltimore, MD 21224, [3]Human Nutrition Research Center on Aging, Tufts University, Boston, MA 02111, [4]Department of Psychology, Towson University, Towson, MD 21252, USA, [5]Departmento de Bioquimica, Instituto de Quimica, Universidade de São Paulo, São Paulo, SP 05508-000, Brazil and [6]Department of Comparative Medicine, University of Washington, Seattle, WA 98195, USA

Received December 21, 2010; Revised April 8, 2011; Accepted April 11, 2011

ABSTRACT

Oxidative DNA damage plays a role in disease development and the aging process. A prominent participant in orchestrating the repair of oxidative DNA damage, particularly single-strand breaks, is the scaffold protein XRCC1. A series of chronological and biological aging parameters in XRCC1 heterozygous (HZ) mice were examined. HZ and wild-type (WT) C57BL/6 mice exhibit a similar median lifespan of ~26 months and a nearly identical maximal life expectancy of ~37 months. However, a number of HZ animals (7 of 92) showed a propensity for abdominal organ rupture, which may stem from developmental abnormalities given the prominent role of XRCC1 in endoderm and mesoderm formation. For other end-points evaluated—weight, fat composition, blood chemistries, condition of major organs, tissues and relevant cell types, behavior, brain volume and function, and chromosome and telomere integrity—HZ mice exhibited by-and-large a normal phenotype. Treatment of animals with the alkylating agent azoxymethane resulted in both liver toxicity and an increased incidence of precancerous lesions in the colon of HZ mice. Our study indicates that XRCC1 haploinsufficiency in mammals has little effect on chronological longevity and many key biological markers of aging in the absence of environmental challenges, but may adversely affect normal animal development or increase disease susceptibility to a relevant genotoxic exposure.

INTRODUCTION

Roughly 400 uracil bases and 10 000 abasic sites have been estimated to be formed per mammalian genome per day due to spontaneous deamination of cytosine or hydrolysis of the *N*-glycosidic bond (1). In addition, attack of DNA by reactive oxygen species, which are generated during normal cellular respiration, results in well over a thousand oxidative base and sugar lesions per day. This enormous load of endogenous DNA damage poses both a mutagenic and cytotoxic threat to the cell, and must be removed in order to preserve genome integrity. Cells have, therefore, evolved a complex array of complementary DNA repair mechanisms that function to recognize and process specific types of DNA damage to restore the genetic code back to its original state. In the absence of efficient DNA repair, individuals exhibit cancer predisposition, susceptibility to neurodegeneration, and other pathologies (2,3). Indeed, a component of the 'free radical (or oxidative stress) theory of aging' proposes that the gradual accumulation of DNA damage over the lifespan of the organism leads to steady cellular decline and eventually organism death (4).

The primary repair system for coping with spontaneous hydrolytic and free radical-induced DNA damage is base excision repair (BER) (5). BER typically involves removal of a base lesion, such as 8-oxoguanine (8-oxo-dG), by a

*To whom correspondence should be addressed. Tel: 410 558 8153; Fax: 410 558 8157; Email: wilsonda@mail.nih.gov
Correspondence may also be addressed to Warren C. Ladiges; Tel: 206 685 3260; Fax: 206 685 3006; Email: wladiges@u.washington.edu

DNA glycosylase, and subsequent incision of the phosphodiester bond at the resulting abasic site by an apurinic/apyrimidinic (AP) endonuclease. Replacement of the missing nucleotide(s) by a gap-filling polymerase is performed either prior to or following DNA termini clean-up, i.e. the generation of a 3′-hydroxyl and 5′-phosphate end. The final step of BER is sealing of the remaining nick by a DNA ligase (6).

X-ray repair cross-complementing protein 1 (XRCC1) is a non-enzymatic scaffold protein that has been suggested to have relevant interactions with several DNA glycosylases, the major human AP endonuclease APE1, the predominant gap-filling DNA polymerase POLβ, and DNA ligase IIIα (7). XRCC1 is a nuclear factor that facilitates repair complex assembly and efficient single-strand break (SSB) resolution, and appears to be excluded from the mitochondria (8). In addition to the interactions above, XRCC1 communicates with several specialized SSB repair proteins, namely polynucleotide kinase/phosphatase (PNKP), tyrosyl-DNA phosphodiesterase 1 (TDP1) and Aprataxin (APTX), which excise frequent 3′ or 5′ blocking groups from DNA, such as 3′-phosphate, 3′-tyrosyl and 5′-AMP residues (9,10). Notably, mutations in *PNKP* have been connected to microcephaly, early-onset, intractable seizures, and developmental delay (11). Mutations in the latter two genes, *TDP1* and *APTX*, are causally linked to the neurodegenerative disorders spinocerebellar ataxia with axonal neuropathy (SCAN1) and ataxia-oculomotor apraxia 1 (AOA1), respectively (12–14). Recent evidence has also suggested a key role for XRCC1 in the protection of neural cells against the genotoxicity of oxidative stress (15), and in neurogenesis of cerebellar interneurons and for hippocampal homeostasis (16). Finally, molecular epidemiology studies in humans indicate that impaired function in XRCC1 may be associated with increased cancer susceptibility (17).

XRCC1 is critical for cell survival upon exposure to agents that generate BER-related DNA damage, such as the alkylating agent methylmethane sulfonate (18), and for suppression of sister chromatid exchange that occurs during S phase as a result of recombinational repair resolution of one-ended double-strand breaks (19). In mice, deletion of both alleles of *Xrcc1* leads to early embryonic lethality, apparently as a result of dysfunctional SSB repair and consequent apoptosis (20). We have employed heterozygous (HZ or $^{+/-}$) mice to explore the consequences of XRCC1 haploinsufficiency on (i) aspects of chronological and biological aging, with a particular focus on brain physiology and (ii) susceptibility to exposure-dependent pathologies.

MATERIALS AND METHODS

Animal background, maintenance and husbandry

For the primary lifespan study and associated analysis (e.g. blood chemistries, behavioral assessments, and imaging), *Xrcc1*$^{+/-}$ mice were rederived from cryopreserved embryos (stock number 000219-EU) that had been deposited by Dr Robert Tebbs and colleagues at the Harlan/Missouri Center of the Mutant Mouse Regional Resource Centers (MMRRC). Three HZ male mice of ~2 months of age were crossed with 2-month-old WT C57BL/6 females (Jackson Laboratories, Bar Harbor, ME) to establish the initial colony. Mice were maintained under standard conditions in a pathogen-free, temperature- and air-controlled barrier environment within a BioBubble enclosure (Fort Collins, CO, USA). Animals were administered Harlan Laboratories (Madison, WI) S2018SX Teklad Global 18% protein extruded rodent diet and provided reverse osmosis water *ad libitum* throughout the course of their lifespan by the NIA Comparative Medicine Section (CMS). Rooms were kept at a 12-h light/dark cycle, maintained at 70–74°F. All animal experiments were carried out according to the 'Guide for the Care and Use of Laboratory Animals' (National Academy Press, USA, 1996) and were approved by the NIA IACUC.

Weights were measured monthly, and overall animal health status was monitored by a designated person within the facility at least every other day, with increased monitoring after the age of 18 months, when signs of morbidity were more likely. Morbidity was used as the lifespan endpoint; to minimize pain and distress, natural death was not an endpoint. Except for those animals found dead unexpectedly, mice were euthanized by CO_2 overdose at the first sign of morbidity. The date of death, and as best could be determined, the cause of death were recorded for all mice in the study.

Genotyping and western blotting

DNA was isolated from mouse tails using a 96-well genomic DNA purification kit from BioPioneer, Inc. (San Diego, CA, USA). The genotype was determined by the NIA Genotyping Lab using isolated DNA and a primer mix of m219 F (AAA CTT CTG GGT CAC CTC TGG ATG), m219 Rwt (CTT AGG ATG GCA GGT TCA AGA CCA) and m219 RNeo (TTG TGC CCA GTC ATA GCC GAA TAG), in a two-step PCR of 94°C for 1 min and 69°C for 2 min for 35 cycles with GoTaq polymerase from Promega (Madison, WI, USA). Amplification of WT chromosomal DNA produced a major PCR product of 484 bp, whereas amplification of HZ DNA generated multiple products of 484 and ~700–800 bp (http://www.mmrrc.org/strains/219/ctr_protocol.pdf).

Western blotting was carried out using the procedure of Lee *et al*. (16). In brief, healthy HZ and WT mice were sacrificed and their cerebellums were removed. The cerebellum was lysed in a prechilled dounce homogenizer in 50 mM Tris, pH 7.5, 200 mM NaCl, 1% Tween 20, 0.2% NP40, 1 mM NaF, 2 mM PMSF, 1 mM activated Na Vanadate, and complete Mini EDTA-free protease inhibitor (Roche, Basel, Switzerland). The lysate was centrifuged (13 000g at 4°C) to remove insoluble material. Thirty microgram of the resulting cell extract was separated on a NuPage MOPS gel (Invitrogen, Carlsbad, CA, USA), and the resolved protein was transferred to a PVDF membrane using standard procedures. A rabbit polyclonal XRCC1 antibody (a kind gift

from Dr Peter McKinnon, St. Jude Children's Research Hospital) was used as the primary antibody, followed by goat anti-rabbit HRP-conjugated secondary antibody (Pierce Biotechnology, Rockford, IL, USA). Detection was carried out using a Pierce Super signal kit. β-actin levels were determined on the same blot to ensure equal loading of protein extracts using a rabbit polyclonal β-actin antibody (Santa Cruz Biotechnology, Santa Cruz, CA, USA) and the same secondary antibody above.

Necropsy and pathological/histological evaluation

Upon death or euthanasia, nearly all animals of the lifespan study were pathologically evaluated using basic necropsy procedures. This evaluation was conducted by an NIA veterinary pathologist or project staff. In addition, two healthy HZ and WT mice (one male and one female for each genotype, all 18.5-month old) were sent to BioReliance (Rockville, MD) for a thorough pathological and histological evaluation of all major organs and tissues. The procedure involved examination and dissection of the animal viscera and carcass as described in BioReliance SOPs. Tissues were collected and fixed in 10% neutral buffered formalin (NBF). The tissues were then processed in the automated tissue processor, embedded in paraffin, sectioned at 6 microns or less, stained with hematoxylin and eosin, and evaluated microscopically. Additional, more targeted pathological and histological evaluation was carried out by BioReliance on three WT male mice (8.75, 10.25 and 23.75 months of age), three WT female mice (8.75, 23.75 and 32.75 months), four HZ male mice (10.25, 15.15 and 26 months) and four HZ female mice (8.75, 23.75, 23.75 and 24 months). These animals were also examined by BioReliance for (i) bone marrow cellularity using the standard brush-smear technique for femurs and (ii) blood cell counts and morphology by manual evaluation of blood smears.

Blood chemistry analysis

A total of 20 mice (five HZ females, five HZ males, five WT females and five WT males) were assessed for a variety of blood chemistries at ~4, 12 and 18 months of age. Blood was collected from animals by retro-orbital techniques into appropriate vials and immediately shipped to BioReliance for analysis. Blood chemistries evaluated included: albumin, alkaline phosphatase, amylase, blood urea nitrogen, creatine, creatine kinase, cholesterol, glucose, triglycerides, aspartate aminotransferase, calcium, direct bilirubin, magnesium, phosphorus, total protein and uric acid. Determination of statistical relevance was performed using ANOVA-single factor.

Behavioral studies

A total of 24 mice (seven HZ females, six HZ males, five WT females and six WT males) were assessed for general activity, motor function and cognitive ability as described below. The same mice were evaluated at each age point to capture within-subject changes across their lifespan. All of the behavioral data were analyzed using ANOVA, followed by Tukey's post hoc comparisons when appropriate.

Open field. To assess general activity, mice were evaluated at 7–8, 13–14 and 19–20 months of age in open fields with automated data collection via photobeam breaks (Med-Associates, St. Albans, VT, USA). Each mouse was tested once at each age indicated. The mice were placed into the open field for 30 min and distance traveled was recorded.

Rotarod. Mice were evaluated at the ages above for motor function and coordination on an accelerating rotarod (Med-Associates, St. Albans, VT). On day 1, the mice were administered a habituation session requiring them to remain on the rotarod moving at a constant speed of 4 rpm for 30 s. The following day each mouse was given three trials, during which the rotarod started at 4 rpm and accelerated to 40 rpm over a period of 5 min. The maximum trial length was 5 min, and there was ~30 min rest period between each trial. The mean across all three trials was determined and used for statistical analysis.

Water maze. In order to assess cognitive function, mice (19–20 months of age) were evaluated in the water maze across 6 days of memory acquisition, with a probe test on Day 7. During the acquisition/retention stage, mice were given four trials per day (60 s maximum) in the maze. Each acquisition trial began with the mouse being placed into the water, facing the wall, at a quasi-random location within the maze (arbitrarily: N, S, E or W). Mice then had to escape onto a hidden platform, which remained in a fixed location across all 6 days of acquisition. Once on the platform, mice were allowed to rest for 30 s before being returned to a holding cage by the experimenter. Mice failing to escape onto the platform within 60 s were placed onto the platform and allowed to remain there for 30 s. For each individual trial, latency, path length and swim speed were recorded using a video tracking system (HVS Image, Buckingham, UK). The inter-trial interval was 40 min. During the probe test on Day 7, the platform was removed and the mice were allowed to swim for 60 s to determine if they would show a preference for the quadrant in which the platform had been located during the acquisition phase.

Magnetic resonance imaging and spectroscopy

Brain imaging and analysis. Experiments evaluating brain morphology and metabolite profile with magnetic resonance imaging (MRI) and spectroscopy (MRS) were performed on six WT (~22 months) and five HZ (~22 months) male mice. Mice were anesthetized with 1.5% isoflurane in a mixture of O_2/air administrated via a face mask, and body temperature was maintained at $36 \pm 1^{\circ}C$ during all procedures. Respiration was monitored using thoracic pressure via an MR-compatible, Model 1025 monitoring and gating system (SA instruments Inc., Stony Brook, NY). Images were acquired on a 7 T/30-cm Bruker spectrometer, using a 35-mm inner diameter whole body resonator for transmission and reception. Multi-slice axial, sagittal and coronal images were

acquired using a moderately T_2-weighted spin echo sequence. MRI parameters included pulse repetition and echo times of TR/TE = 710 ms/26.5 ms, number of shots per acquisition of NEX = 2, field of view of FOV = 3.0 × 3.0 cm, slice thickness = 1.0 mm and matrix size 256 × 128. The cerebellar volume was computed by manually tracing the contour encompassing the cerebellar tissue within each slice of the stacked images for each mouse.

Brain spectroscopy. Localized water-suppressed ^{1}H spectra of the central cerebellum (voxel dimension $4 \times 2.5 \times 1.5$ mm^3) were obtained by using the point resolved spectroscopy (PRESS) sequence, with TR/TE = 2.5 s/135 ms, 160 signal averages, 1024 data points with a spectral range of 10 ppm and a total scan time of ~7 min. The given value for TE was selected to provide a degree of spectral editing, permitting more unambiguous resonance quantification. *N*-acetyl aspartate (NAA) was quantified as a marker for neuron viability, with choline (Cho) used for normalization. Statistical analysis was performed using a two-tailed Student's *t*-test, with $P < 0.05$ considered significant. Data are presented as mean ± standard deviation (SD).

Imaging of abdominal fat and analysis. MRI was used to evaluate abdominal fat in five WT (~22 months) and five HZ (~22 months) female mice as described above for brain imaging. A moderately T_1-weighted spin echo sequence was used, with and without VAPOR fat suppression (21). Parameters included TR/TE = 390 ms/13.2 ms, NEX = 2, FOV = 4.0 × 4.0 cm (fat axial imaging) or 5.0 × 4.0 cm (fat sagittal and coronal imaging), 1.0 mm slice thickness, and 256 × 128 matrix size. Adipose tissue was quantified using ImageJ (22), according to the following procedure. Image processing was performed by first multiplying fat-suppressed and non-suppressed images to enhance contrast, and then applying an unsharp mask to enhance edge definition. Segmentation into adipose and non-adipose tissues was then implemented through k means clustering. Subcutaneous and intra-abdominal adipose tissues were manually delineated within each slice of the stacked images for each mouse to permit measurement of their respective volumes.

Chromosome aberration analysis

Two WT and 2 HZ male mice (~26 months of age) were injected with 0.1 cc of 0.5% colchicine intraperitoneally. After 30 min period, animals were euthanized and the femur was removed. Cells were flushed—following distal puncture of the bone—into a 15 ml tube using a 1 cc syringe filled with 0.56% KCl. Cells were incubated for 15 min at 37°C and then harvested at 400*g* for 5 min. The supernatant was removed and discarded, and 0.5 ml of fixative (3:1 methanol:glacial acetic acid) was added without disturbing the pellet. After a brief incubation in fixative, the solution was removed and replaced with fresh fixative. To prepare chromosome spreads, an aliquot of the above bone marrow cells was dropped on a clean slide and allowed to air dry. Subsequently, chromosomal DNA was stained with Vector Vectashield (Burlingame, CA, USA) Hardset Mounting Medium with DAPI. Samples were covered with a cover slide and allowed to set overnight away from light. Visualization of chromosome spreads was performed with an Olympus (Center Valley, PA, USA) Axiovert microscope at 100× magnification. Metaphase spreads were evaluated for chromosome number and abnormalities for each animal.

Telomeric fluorescence *in situ* hybridization (telomeric-FISH)

Metaphase spread preparation was carried out as above. Telomeric-FISH was performed as previously described (23), using Cy-3-labeled $(CCCTAA)_3$ protein nucleic acid (PNA; Applied Biosystems, Foster City, CA,USA) as a probe. Metaphases were examined for telomere abnormalities, including telomere signal free ends and chromosome end-to-end fusions, with a Zeiss (Jena, Germany) Axiophot fluorescence microscope.

Bone marrow cell viability assay

Bone marrow cells were harvested from the femurs of two HZ and two WT 4-month-old male mice essentially as described above, but were grown in Iscove's Modified Dulbecco's medium (IMDM) containing murine stem cell factor [MSF at 100 ng/ml (Peprotech, Rocky Hill, NJ, USA)] and recombinant murine interluekin-6 [IL-6 at 200 U/ml (Peprotech, Rocky Hill, NJ, USA)]. After culturing in media for 24 h at 20% O_2/5% CO_2, cells were counted and split into either 96-well plates (cell viability assay) or 6-well plates (chromosome analysis). For the cell viability assay, cells were plated at 1×10^4 cells per well in replicates of five. The cells were allowed to grow for 24 h as above, and then exposed to various concentrations of MMS (0, 0.3, 1, 3 or 10 mM) for 1 h. Cells were then washed three times with 1× PBS, and grown for an additional 48 h in IMDM supplemented with MSF and IL-6. Cell viability was determined using the cell proliferation reagent WST-1 (Roche, Indianapolis, IN) following the manufacturer's standard procedure. In short, cells (in 100 µl IMDM medium) were incubated with 10 µl of WST-1 reagent for 1 h and evaluated using a BioRad (Hercules, CA) Benchmark Plus microplate spectrophotometer and Microplate Manager Software. A dual wavelength (450 and 650 nm) protocol was used to determine the absorbance of the samples. *Ex vivo* chromosome analysis was carried out as described above, with the following modification. Instead of injecting colchicine into the mice, colchicine (10 µg/ml) was added to the IMDM media 24 h post-plating of a six-well plate (cell density of 1×10^5 cells per well). Cells were allowed to grow in the presence of colchicine for 5 h at 20% O_2/5% CO_2 before preparation of chromosome spreads.

Treatments with high fat-diet or azoxymethane

Mice used in the two treatment paradigms [i.e. high-fat diet (HFD) or azoxymethane (AOM) exposure] were obtained and maintained as for the lifespan study. These animals were maintained in ventilated cages (less than five per cage) in a specific pathogen free facility at the

University of Washington. Mice were fed standard chow (except for the HFD) and provided reverse osmosis water. Rooms were kept at a 12-h light/dark cycle, maintained at 70–74 F, 45–55% humidity with 28 changes per hour. Mice were genotyped using similar procedures as for the lifespan study.

In the HFD studies, 15 HZ and 15 WT mice were maintained on standard rodent chow (5053, Picolab, Richmond, Indiana) containing 20% (wt/wt) protein, 4.5% fat (ether extract) and 55% carbohydrate (primarily starch) beginning at the time of weaning. At 16 weeks of age, ten mice of each genotype were switched to a high-fat, high-sucrose (high caloric) diet (S3282; Bio-Serv, Frenchtown, NJ, USA) containing 20% protein, 36% fat (primarily lard) and 36% carbohydrate (primarily sucrose) for 12 weeks. Food intake was measured every 3 weeks. Two to three mice of the same genotype were housed per cage, and food intake was measured as the weight of food per cage consumed over a 24-h period, averaged between the number of mice in each cage. Food was weighed three times in a row over the course of 3 days, and averaged.

To evaluate the susceptibility of *Xrcc1*$^{+/-}$ mice to AOM-induced pathologies, 4-month-old HZ and WT male littermates ($N = 13$ and 15, respectively) were injected with 10 mg/kg AOM (Sigma cat# A2853) intraperitoneally, once a week for six weeks. Three mice of each genotype were injected with sterile diluent. All mice were monitored and weighed weekly and terminated 6 weeks following the last injection. Livers were grossly staged for lesion severity, and sections collected. Colons were removed and flushed with ice cold phosphate-buffered saline, opened and stained with methylene blue. The entire length of colon was used to count aberrant crypt foci using a dissecting microscope. Liver and representative colon sections were fixed in 10% neutral buffered formalin and subsequently stained with hematoxylin/eosin for histopathological evaluation.

Histopathological scoring of the liver was based on: Grade 1, no evidence of toxicity; Grade 2, mild focal hepatocellular necrosis, with limited evidence of mild focal hepatocellular hyperplasia and hypertrophy, mild focal bile duct hyperplasia and perivascular infiltration of mononuclear inflammatory cells consisting of lymphocytes and macrophages; Grade 3, moderate focal hepatocellular hyperplasia and hypertrophy with pyknotic nuclei and hepatocyte necrosis, moderate focal bile duct hyperplasia and perivascular infiltration of lymphocytes and macrophages, and occasional fibroblasts; and Grade 4, areas of extensive necrosis replaced by severe, multifocal nodular hepatocellular hyperplasia and hypertrophy with hepatocytes showing enlarged cytoplasm and mild vacuolation, karyomegaly, and marked variation of nuclear size with multiple nucleoli. Grade 4 also included:locally extensive multifocal biliary hypertrophy and hyperplasia with marked biliary dilation and periductal infiltrates of lymphocytes and macrophages; and severe, multifocal, periportal infiltrates of mononuclear inflammatory cells with an increased number of fibroblasts suggestive of early fibrosis.

RESULTS

Crosses between C57BL/6 *Xrcc1*$^{+/-}$ males and females recapitulated the reported inviability of homozygous knockout mice (20), as no null animals were observed among the 27 pups genotyped (unpublished observation). Given the incompatibility of deletion of both alleles of *Xrcc1* with life, we evaluated herein the impact of XRCC1 heterozygosity on chronological and physiological aging parameters without exposure, and on disease susceptibility in the face of altered diet or an exogenous challenge. The haploinsufficient animal model may very well recapitulate the reduced XRCC1 function phenotype that apparently exists in the human population (24,25).

XRCC1 heterozygosity

We confirmed that *Xrcc1*$^{+/-}$ animals expressed reduced levels of XRCC1 protein. Specifically, western blot analysis of extracts prepared from the cerebellum of 1-month-old mice showed that HZ animals expressed slightly <50% of XRCC1 protein relative to the WT counterparts (Figure 1A). Quantitative RT-PCR of total RNA and western blot analysis of extracts from spleen of 6 to 10-month-old animals also revealed roughly 60% transcript and 60% protein in the HZ mice (data not shown; Dr Patricia Gearhart, National Institute on Aging, personal communication). In addition, we had demonstrated previously that isolated *Xrcc1*$^{+/-}$ primary cerebellar granule cells exhibited increased DNA strand break accumulation and apoptotic cell death following menadione exposure relative to cells from WT littermates, further supporting reduced XRCC1 activity (15). Collectively, these results demonstrate that loss of one allele of *Xrcc1* results in reduced expression of XRCC1 in mice and cellular susceptibility to exogenous genotoxin exposure (see also later).

Lifespan of HZ animals:chronological aging

As a general means of assessing the impact of XRCC1 haploinsufficiency on mouse health and longevity, we determined the lifespan and, where possible, the cause of death of 82 WT (44 male and 38 female) and 92 HZ (51 male and 41 female) C57BL/6 animals. As evident from the data presented in Figure 1B, an XRCC1 deficiency had no significant effect on the median life expectancy (~790 days), despite the early deaths of a subset of HZ animals (see below), or the maximal lifespan of the animal, a conclusion that was not altered when the data was broken into male and female categories (1153 days for the longest lived WT male, 1168 days for the HZ male, 1162 days for the WT female and 1171 days for the HZ female).

When cause of death was evaluated, some differences were noticed between genotypes. In particular, HZ males and females (total of seven) showed a propensity for abdominal organ rupture, which we have defined in this study as splitting of the organ within the abdominal cavity, that was not seen in the WT counterparts (Table 1, $P = 0.01$). Specifically, ruptures of the bladder (two cases, one male at 6 months and one female at 2 months), liver (one case, male at 7 months) and pancreas (four cases, two

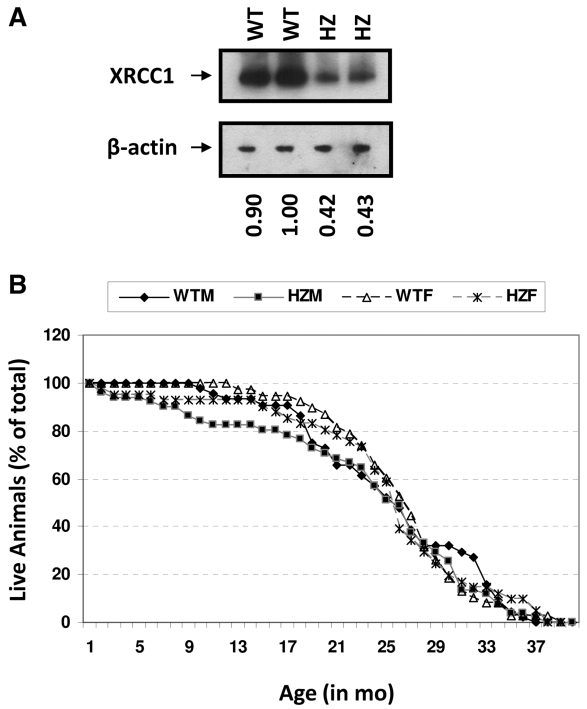

Figure 1. (**A**) Western blot analysis. Two HZ and two WT cerebellar extracts were analyzed via western blot analysis. Top: An anti-XRCC1 rabbit polyclonal antibody was used as the primary antibody. Bottom: β-actin levels were measured to ensure equal loading of lanes. The XRCC1: β-actin ratio [determined from a scanned image of the western blot autoradiograph using ImageQuant software (GE Healthcare, Piscataway, NJ)] normalized to the WT extract denoted 1.0 is indicated below each lane. (**B**) Lifespan plot. Percentage of mice alive is plotted against age in months for WT male (WTM), WT female (WTF), HZ male (HZM), and HZ female (HZF). Total animals per group were as follows: 82 WT (44 male and 38 female) and 92 HZ (51 male and 41 female).

Table 1. Cause of death (COD)

Mouse genotype and gender	COD						
	Infection	Tumor	ND	Abdominal issue		Other	
				A*	B	C**	D
WTM (44)	6	14	19	0	3	0	2
WTF (38)	7	6	22	0	2	0	1
HZM (51)	6	5	30	4	2	2	2
HZF(41)	5	6	18	3	4	1	4

The total number of animals for each genotype (wild type = WT, heterozygous = HZ) and gender (male = M, female = F) are indicated in parentheses to the left. The number of animals for each COD classification is also indicated. A = organ rupture, B = autolysis, C = neurological and D = other (malocclusion, prolapse, etc.). ND = not determinable (or natural). Chi-square contingency table analysis: $*P = 0.01$, $**P = 0.1$.

males at 7 and 9 months and two females at 2 and 7 months) were diagnosed. These ruptures caused large amounts of blood and fluid to be released into the abdominal cavity and in some cases resulted in autolysis. In none of the situations, however, was it clear whether the rupture was due to a structural instability in the tissue of the organ wall, a hemorrhaging of the organ's blood vessels, or another cause.

HZ males and females (total of three) also showed a few life-shortening complications related to possible neurological deficits that were not seen in the WT colony (Table 1, $P = 0.1$). In particular, two cases of 'head tilting to one side' (one HZ male, 21 months and one HZ female, 26 months) and one case of 'impairment of lower leg movement on one side of body' (HZ male, 26 months), behaviors commonly associated with a stroke, were observed.

The tumors observed during necropsy in the animals of the lifespan study (Table 1) included several types, although none were confirmed through histological evaluation. In WT males, six histocytic sarcomas, five hepatocellular carcinomas, two thoracic tumors and one urinary carcinoma were detected. In WT females, three histocytic sarcomas, two hepatocellular carcinomas, and one ovarian cancer were observed, as was a case of general metastasis without a known precursor. In HZ males, three histocytic sarcomas and three hepatocellular carcinomas were seen. In HZ females, three histocytic sarcomas, one lymphoid tumor, and one case of general metastasis without known precursor was recorded. Although there is an apparently statistically significant lower tumor frequency in the HZ males relative to the WT males ($P = 0.007$, Chi-square contingency table analysis), independent confirmatory studies are needed to conclude that XRCC1 deficiency has a beneficial effect on sex-dependent spontaneous cancer risk.

Physiological aging of HZ animals

We also assessed the following measurable end-points to determine the effect of *Xrcc1* heterozygosity on the animal's physiological age or condition.

Histology. An extensive necropsy was performed on two healthy HZ and WT mice (one male and one female for each genotype at 18.5 months of age) as described in 'Materials and Methods' section. Upon preparation, the following tissues were evaluated and found to exhibit normal histological morphology regardless of genotype and sex: lung, thymus, spleen, liver, kidney, heart, trachea, ileum, cecum, colon, brain with middle ears and nasal cavity with eyes (data not shown).

In light of the organ ruptures noted above, which may stem from developmental abnormalities during endoderm or mesoderm formation, an additional set of animals were analyzed (three WT males, three WT females, four HZ males and four HZ females; see 'Materials and Methods' section) and the integrity of relevant tissues evaluated, such as the pancreas and thyroid. Pathological and histological analysis, which included examination of the liver, spleen, heart, brain, lung, testes/ovaries and bone marrow/femur, in addition to the pancreas and thyroid, found that all animals exhibited normal histopathology in line with their age. Analysis of these 14 mice indicated three cases of cancer: histiocytic sarcoma was noted in two of the WT

animals (females, 23.75 and 32.75 months) and alveolar bronchiolar adenoma was noted in another WT mouse (male, 23.75 months). All of these cancers, as well as several other non-neoplastic lesions observed in some of the 14 animals, are considered spontaneous/background findings typical for any strain of mouse.

In all but one (WT, female, 32.75 months) of the 14 animals, bone marrow analysis revealed normal cellularity and a heterogeneous population, with erythroid, myeloid and megokaryocyte precursors present and in adequate number. In the case of the aberrant animal, a population of pleomorphic neoplastic cells with large variable nuclei and abundant cytoplasm (i.e. suggestive of a malignancy of undetermined origin) was identified; this population is most likely attributable to the histiocytic sarcoma diagnosed in multiple organs in this WT female mouse. For the manual complete blood count (CBC) analysis, there was no difference in the composition or morphology of the various blood cell types (neutrophils, basophils, eosinophils, lymphocytes and monocytes), which were found to be within the normal limits, with the exception of the WT female mouse (23.75 months) noted earlier. This particular animal showed markedly poor cellularity with rare lymphocytes and neutrophils present, most likely due to the neoplasm outlined above.

Weight. Previous studies have suggested a possible involvement of BER in obesity, dyslipidemia and fatty liver disease, as a deficiency in the DNA glycosylase NEIL1 results in a physiological state that mimics human metabolic syndrome (26). As seen in Figure 2, mice gained weight in an age-related manner up to ~20 months of age. The *Xrcc1*$^{+/-}$ animals, independent of gender, displayed no obvious weight differences at any age relative to the age-matched WT controls.

We previously demonstrated that a HFD given to young adult male mice on a C57BL6 genetic background can simulate an age-related weight gain (caused by an increase in fat mass), as well as increase inflammatory stress and down-regulate XRCC1 expression in intestinal

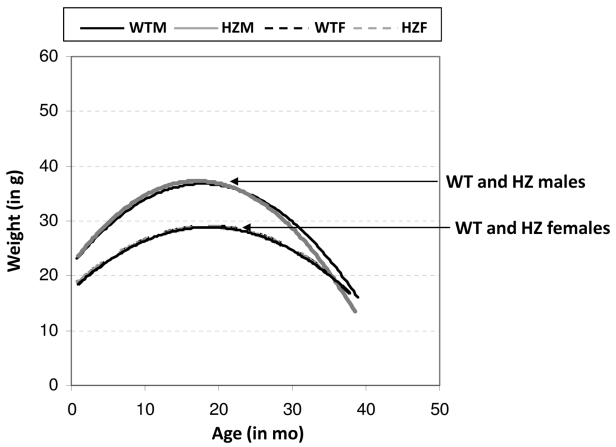

Figure 2. Weight plot: Weight in grams is plotted (using polynomial line of best fit) against age in months for WTM, WTF, HZM and HZF. Each line is comprised of 371–427 data points, including 2–20 measurements for each of the 174 animals during their lifespan.

polyps [(27) and unpublished data]. We hypothesized that HZ mice might be sensitive to a HFD, since levels of XRCC1 protein are diminished. After 12 weeks on the HFD starting at four months of age, HZ mice gained an average of 13 gm (29% increase) compared to WT mice, which gained an average of 10 g (23% increase) with no statistical difference. These observations agree with the similarity in body weights of the different genotypes of old mice, and re-affirm that obesity is not related to XRCC1 haploinsufficiency.

Blood chemistries. To assess the overall health status, as well as the functions of various organs in the HZ mice, a series of blood chemistry tests were performed at 4, 12 and 18 months of age. Parameters analyzed included: albumin, alkaline phosphatase, amylase, blood urea nitrogen, creatine, creatine kinase, cholesterol, glucose, triglycerides, aspartate aminotransferase, calcium, direct bilirubin, magnesium, phosphorus, total protein and uric acid. For nearly all measurements, HZ mice exhibited statistically similar values to those determined for the age-matched WT counterparts at each life stage (Supplementary Table S1). The possible exceptions for the HZ animals included elevated albumin (ALB, *P*-values: 0.00013—males; 0.009—females) and creatine phosphokinase (CPK, *P*-values: 0.004—males; 0.14—females) at 12 months, and although statistically insignificant, apparent trends for decreased bilirubin at 4 months (DBL), and elevated blood urea nitrogen (BUN) and phosphorus (PHOS) primarily in the older mice.

Behavioral attributes. Given the association between defects in SSB repair and neurological abnormalities (10), we examined the impact of *Xrcc1* heterozygosity on brain function by evaluating: general activity levels, gross locomotor activity and exploration habits (via open field); motor coordination, balance and equilibrium (via rotarod); and spatial memory (via water maze). In the open field there were no genotype differences for distance traveled, but there was an overall decrease at 19–20 months of age ($F_{(2,38)} = 14.33$, $P < 0.001$; Figure 3A). Evaluation of motor function and coordination indicated no statistically significant differences between sex-matched WT or HZ animals, although there was a consistent trend at each age analyzed for the HZ males to exhibit reduced time on the rotarod (Figure 3B). An expected, overall decrease in the ability of all animal categories to remain on the accelerating rotarod was seen with age ($F_{(2,38)} = 15.02$, $P < 0.001$).

For the water maze, there was a general effect of'days of training' for latency ($F_{(5,100)} = 23.25$, $P < 0.001$) and path length ($F_{(5,100)} = 32.37$, $P < 0.001$), indicating that all mice, regardless of genotype, were able to learn (Supplementary Figure S1A and B). However, there was no statistically significant difference between the various groups for either of these measures at any of the days of acquisition. There were also no group differences for swim speed, indicating that there was no XRCC1-dependent effect on aptitude to perform in the water maze (Supplementary Figure S1C). For the probe test, there was no disparity between the groups in their preference

to search the quadrant in which the platform had been located during acquisition ($F_{(9.60)} = 1.36$, $P = 0.225$), indicating that both WT and HZ animals were able to learn and remember the location of the hidden platform equally well (Supplementary Figure S1D).

Organ and tissue status. Again, given the reported association of SSB repair defects with neurodegeneration, and since the rotarod studies herein suggested a possible impairment in motor coordination for HZ male mice (Figure 3B), we employed MRI and MRS studies on age-matched WT and HZ male animals to determine relative brain dimensions and volume, and brain metabolite (NAA:Cho) ratios, the latter of which permits an assessment of local neuronal viability and function. In addition, since prior studies suggested a role for BER defects in obesity (26), we employed MRI to determine intra-abdominal fat (IAF) and subcutaneous fat (SF) in age-matched WT and HZ female mice.

Figure 4A shows the results of brain MRI and MRS performed on six WT and five HZ ~18-month-old male mice. Typical image slices are shown along the three orthogonal axes, as well as a typical spectrum obtained from the indicated voxel (Figure 4A, left). No statistically significant difference was observed in cerebellum volume between the WT and HZ age-matched groups (Figure 4A, right). For the MRS study, high-quality PRESS-localized ^{1}H spectra were obtained with the selected value of TE = 135 ms, which permitted editing of lipid and clear delineation of the resonances for choline, creatine and NAA (Figure 4A, lower left panel). No difference in neuronal viability was identified between the WT and HZ age-matched male animals as measured by the NAA/Cho ratio (WT, 0.90 ± 0.32; HZ, 0.88 ± 0.42). We note that for both MRI volume and MRS measurements of neuronal viability, a larger variability in the data was seen with the *Xrcc1*$^{+/-}$ animals.

Abdominal MRI was performed on six WT and five HZ ~22-month-old female mice. Typical coronal (top) and axial (bottom) slices with T_1-weighting are shown in Figure 4B (left). The volumes of IAF and SF for individual mice were determined from image segmentation along axial, sagittal and coronal sections and averaged. Results normalized individually by body weight (Figure 4B, right) revealed no statistically significant difference between groups for total fat (IAF + SF) (WT: 157.3 ± 59.9 mm^3/g; HZ: 169.3 ± 84.4 mm^3/g) or IAF (WT: 79.0 ± 30.7 mm^3/g; HZ: 83.5 ± 39.7 mm^3/g). The two experimental groups also did not differ in total fat or intra-abdominal fat

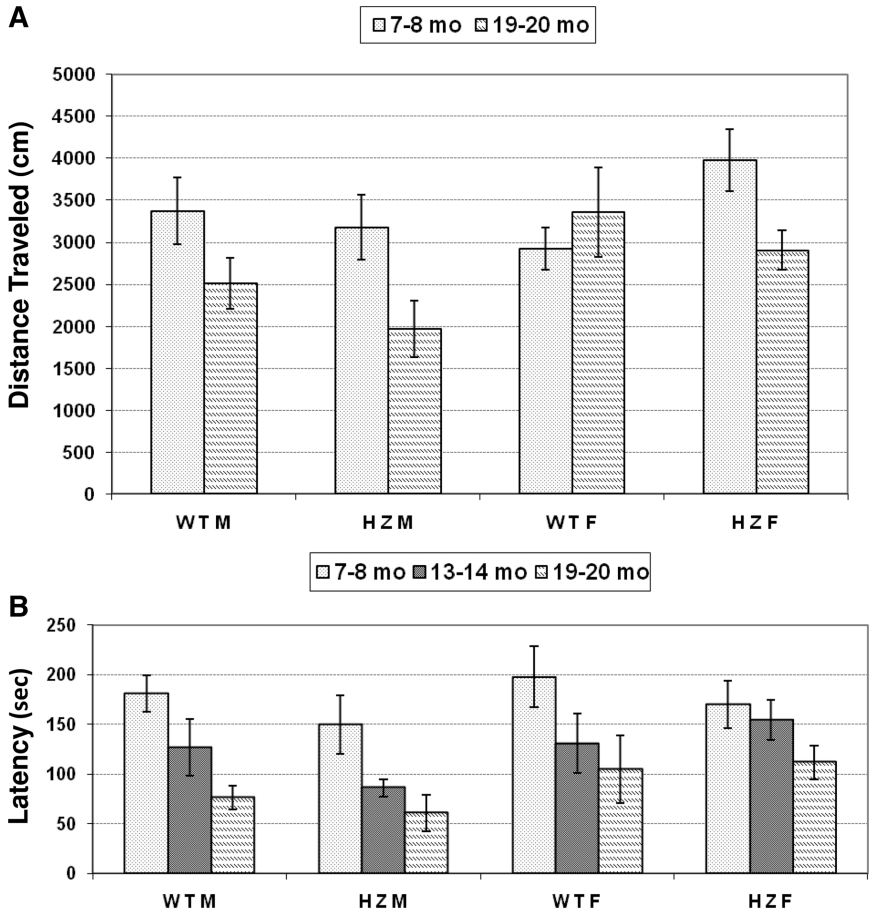

Figure 3. Open field and rotarod analysis. (**A**) Mean distance traveled (± SEM) in the open field during 30 min sessions evaluated at 7–8 or 19–20 months of age for WTM, WTF, HZM and HZF mice. (**B**) Mean latency (± SEM) to fall from the accelerating rotarod when evaluated at 7–8, 13–14 or 19–20 months of age.

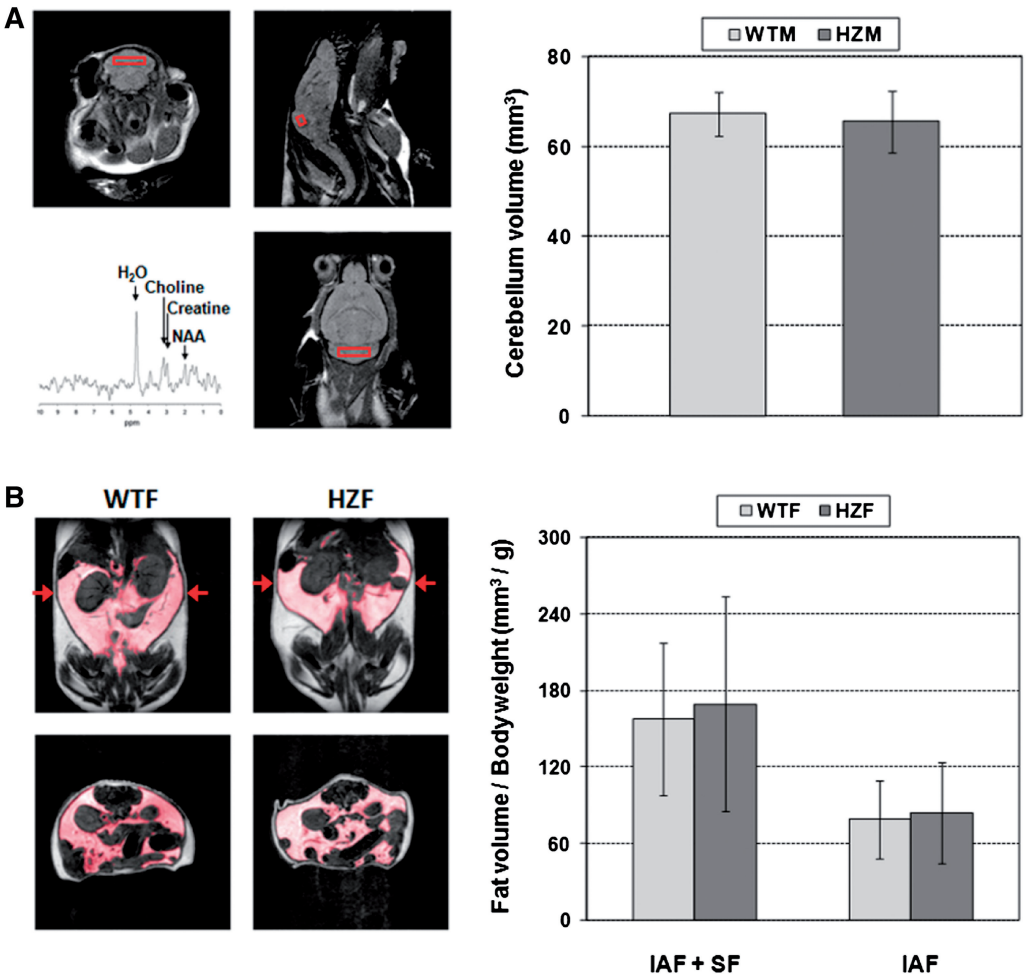

Figure 4. Brain and fat imaging. (**A**) MR brain imaging and spectroscopy. Left: T_2-weighted axial (upper left), sagittal (upper right) and coronal images (lower right) through the cerebellum of an *Xrcc1*$^{+/-}$ male mouse. Proton spectrum (lower left) acquired from the indicated voxel (PRESS localization; TE = 135 ms) as used to quantify the NAA/choline ratio (see text). Right: Cerebellar volumes for the WT (67.3 ± 4.9 mm^3) and HZ (65.5 ± 6.8 mm^3) male mice. (**B**) Abdominal fat imaging. Left: T_1-weighted MR images without fat suppression acquired from a WT female (left column) and a HZ female (right column), respectively. The position of the axial slices (bottom row) is as indicated by the arrows shown in the coronal slices (top row). Fat is bright in these images, with the shaded region indicating IAF and the remaining region SF or intra-muscular fat. Right: Quantification of total fat per body weight among the mice examined.

when quantified without normalization by body weight (data not shown).

Effect of *Xrcc1* heterozygosity on spontaneous genomic instability *in vivo*

To assess the effect of *Xrcc1* heterozygosity on genetic stability *in vivo*, bone marrow cells were isolated from WT and HZ 26-month-old mice (two each) following intraperitoneal administration of colchicine and examined for spontaneous chromosome and telomere abnormalities. Specifically, metaphase spreads were evaluated for chromosome number and overall integrity, i.e. breakage, fragmentation, or other gross chromosomal rearrangements, as well as telomere signal free ends or end-to-end fusions. These studies revealed that *Xrcc1*$^{+/-}$ mouse cells show no obvious chromosomal or telomere alterations (Supplementary Figure S2, Table 2, and data not shown), suggesting that XRCC1 heterozygosity has no effect on spontaneous genomic instability. This conclusion was supported by the fact that HZ bone marrow cells displayed a normal cell cycle profile with 2N DNA content as assessed by fluorescence activated cell sorting (FACS) analysis (data not shown).

Analysis of bone marrow cells isolated from two additional WT and HZ male mice (4 months of age) found no overt chromosome abnormalities, including fragmentation, breakage or fusions, following culturing and treatment with colchicine *ex vivo* (data not shown). Aneuploidy was observed in 3 of 49 and 8 of 48 metaphase spreads from the two WT mice, and 9 of 48 and 9 of 46 from the HZ animals ($P = 0.13$ when comparing the combined results; Chi-square contingency table analysis), further supporting no statistically significant difference in chromosome stability between the two genotypes.

Exposure-dependent sensitivity of *Xrcc1*$^{+/-}$ bone marrow cells

Xrcc1$^{+/-}$ mice did not show any gross phenotypes in comparison to WT mice by several measurements (see above), suggesting that the single functional *Xrcc1* allele or other backup DNA repair pathways can cope with natural, spontaneous DNA damage. We next determined whether an *Xrcc1*$^{+/-}$ state was sufficient to handle the increased DNA damage expected upon exposure to an exogenous genotoxin. Towards this end, primary bone marrow cells were isolated from two WT and two HZ littermates and challenged with varying doses of the alkylating agent MMS. As shown in Figure 5, HZ cells exhibited a statistically significant reduction in viability at 1, 3 or 10 mM MMS relative to WT controls, indicating a dose-dependent sensitivity of XRCC1-deficient cells to a relevant genotoxin.

Table 2. Chromosome number (aneuploidy) in WT and HZ *Xrcc1* bone marrow cells

Mouse ID No./Genotype	No. of metaphase counted	No. of aneuploid cells	Percentage of aneuploid cells
NTH574/WT	58	5	8.6
NTH834/WT	57	1	1.8
NTH567/HZ	47	5	10.6
NTH575/HZ	62	3	4.8

Percentage of aneuploid cells per at least 47 metaphases examined is shown.
Note: No gross structural chromosome abnormalities were seen in either the WT or HZ background (data not shown). Chi-square contingency table analysis of the combined data (6 of 115 for WT, 8 of 109 for HZ) reveals $P = 0.51$.

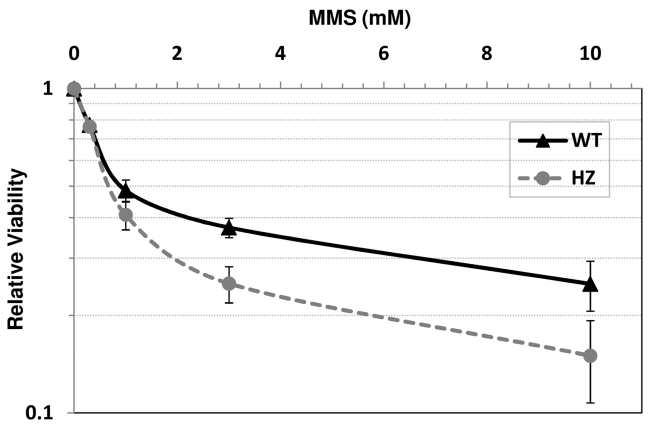

Figure 5. Cell viability following MMS exposure. Bone marrow cells were isolated from two WT and two HZ animals, cultured at 20% O_2/5% CO_2 in IMDM supplemented with MSF and IL-6, and then challenged with 0, 0.3, 1, 3 or 10 mM MMS. Following treatment, cells were cultured as above for an additional 48 h, WST-1 reagent was added to the medium for 1 h, and the absorbance was measured. Shown are the average and standard deviations at each treatment regime of a total of six data points (two mice, three data points each). Single factor ANOVA analysis determined *P*-values of 0.55, <0.01, <0.0001 and <0.01 at 0.3, 1, 3 and 10 mM MMS, respectively.

Exposure-dependent susceptibility of HZ animals

Given the increased sensitivity of *Xrcc1*$^{+/-}$ bone marrow cells to MMS, we evaluated the susceptibility of HZ mice to exposure-dependent pathologies, employing the alkylator AOM, in order to replicate a potential environmental challenge. AOM is a pro-carcinogen that is metabolized by cytochrome P450 to methylazoxymethanol, a chemical intermediate that breaks down to formaldehyde and a highly reactive alkylating species, likely methyldiazonium (28). AOM is known to generate alkylated base adducts in DNA, such as N^7-methylguanine and O^6-methylguanine, the latter of which drives G to A transition mutations. This compound is routinely used experimentally to induce tumorigenesis in the colon of laboratory animals, and thus, to study the mechanism of cancer progression and chemoprevention. When *Xrcc1*$^{+/-}$ mice were necropsied 12 weeks after first starting the AOM exposure, grossly observable liver lesions were seen in all 13 HZ mice, but were present in only five of 15 WT littermates. The lesions consisted of modular, multifocal areas of discoloration, which upon histological examination were areas of necrosis, hepatocellular hyperplasia, biliary hyperplasia and hypertrophy, and perivascular inflammation (Figure 6A). When assigned a grade of 1–4 (see 'Materials and Methods' section), livers from *Xrcc1*$^{+/-}$ mice had a score of 3.1 ± 0.6, while livers from WT littermates had a score of 1.3 ± 0.5 ($P \leq 0.05$) (Figure 6B). In the colon, staining with methylene blue showed large numbers of aberrant crypt foci, 38 ± 5 per HZ mouse, compared to only 15 ± 2 for WT mice. Occasional adenomatous polyps were seen in HZ mice, but not in WT mice (data not shown). Based on these findings, we conclude that *Xrcc1*$^{+/-}$ mice are haploinsufficient for the toxic and pre-cancerous affects of the DNA-damaging agent AOM.

DISCUSSION

XRCC1 is a non-enzymatic scaffold protein that facilitates efficient SSB repair and has been associated with neurodegenerative disease and cancer susceptibility (10,17,29). Using *Xrcc1*$^{+/-}$ mice, we evaluated longevity and a series of endpoints related to health span, primarily in the absence of exposure. In all, XRCC1 haploinsufficiency had no overt effect on animal life expectancy, weight, organ function (as assessed by various blood chemistries), motor coordination, brain integrity or memory, body fat composition, bone marrow cellularity, blood cell composition or morphology, or chromosome status. The generally normal phenotype of the HZ mice, including the lack of an obvious increase in spontaneous neoplasms and the intact chromosome structure, indicate that ~50% XRCC1 protein is largely sufficient to maintain normal animal fitness and genome integrity in a controlled, toxin-free environment. The two most noticeable consequences of *Xrcc1* heterozygosity were a propensity for early death, primarily due to abdominal organ rupture, and an increased susceptibility for liver toxicity and precancerous lesions in the colon when challenged with an exogenous agent, i.e. the alkylator AOM.

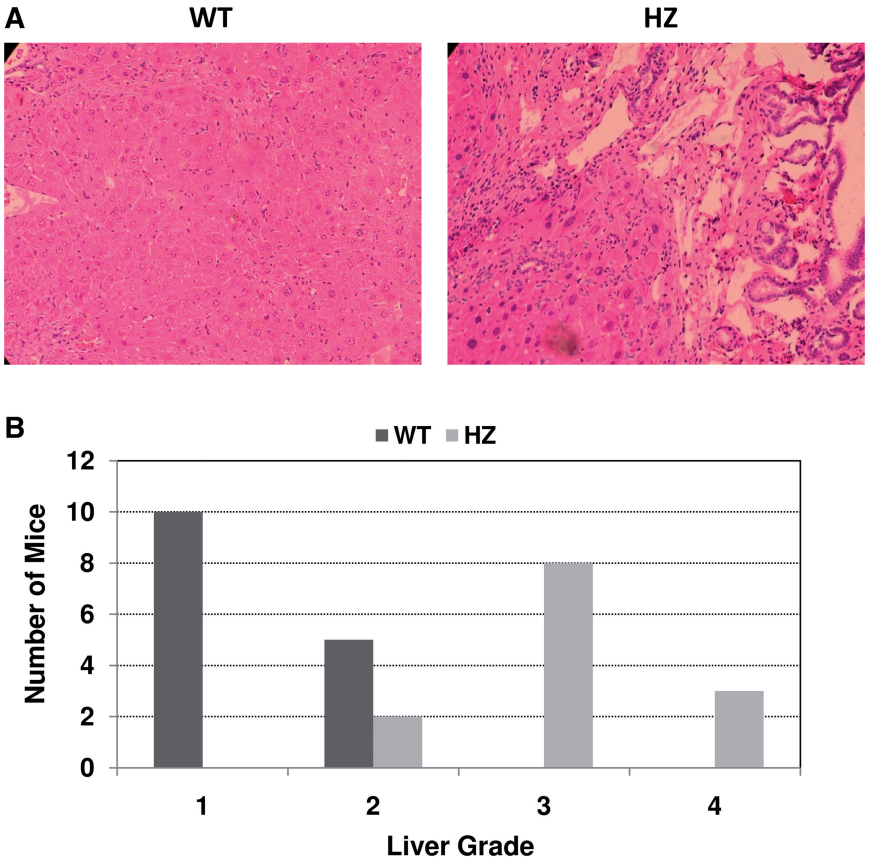

Figure 6. AOM-induced liver toxicity. (**A**) Liver from an *Xrcc1*$^{+/-}$ (HZ) mouse shows areas of necrosis and severe multifocal hepatocellular hyperplasia and hypertrophy, mild vacuolation, karyomegaly, and marked variation of nuclear size with multiple nucleoli. There was moderate locally extensive multifocal biliary hypertrophy and hyperplasia with biliary dilation and periductal and periportal infiltration of mononuclear inflammatory cells, and variable numbers of fibroblasts. Liver from a WT littermate shows some evidence of focal hepatocellular necrosis, with mild hepatocellular hyperplasia and hypertrophy, and limited perivascular infiltration of mononuclear inflammatory cells. (**B**) Number of HZ and WT mice in each of the different histopathological liver grades (1–4, see 'Materials and Methods' section).

Although the exact cause of death was undeterminable in many cases (Table 1), we did observe an occasional abdominal organ rupture exclusively in HZ male and female mice at a relatively young age (2–9 months). This outcome may be related to the essential role that XRCC1, and presumably BER, plays in embryonic development (20,30). In particular, a characteristic of *Xrcc1* null (*Xrcc1*$^{-/-}$) E6.5 and E7.5 embryos was an abnormal morphology of the embryonic endoderm, a germ layer that ultimately gives rise to the epithelium of the gastrointestinal and respiratory tracts, as well as major endocrine glands and organs (e.g. the liver and pancreas). Other extraembryonic tissues including the parietal endoderm, extraembryonic ectoderm, ectoplacental cone and trophoblast giant cells appeared healthy in *Xrcc1*$^{-/-}$ embryos, albeit somewhat smaller than normal (20). More detailed analysis indicated that the lineage-specific abnormalities correlated with the amount of unrepaired DNA damage as detected by the alkaline Comet assay (20). These observations may suggest that individuals with a defect in a critical DNA repair process, such as SSB repair, will be more prone to congenital gastrointestinal malformations or other diseases, for example, of the lung, liver or pancreas.

It is becoming more appreciated that the developmental dynamics and the final integrity of the nervous system require vigilant DNA repair processes from the beginning, particularly during the early period of rapid proliferation when progenitor cells are expanding and differentiating to generate the complex neural network (31). While our data did not reveal an overt effect of *Xrcc1* heterozygosity on neurogenesis or brain function, suggesting sufficient SSB repair or compensatory pathways to cope with spontaneous, endogenous DNA damage, there appeared to be neurological involvement in some of the animals (Table 1). In fact, the behavior observed in three HZ mice (i.e. head tilt and impairment of lower leg movement) is seemingly in line with evidence implicating XRCC1 in modulating the cerebral response to ischemia and the risk of stroke in rodents and humans (32–35). Consistent with XRCC1 and SSB repair playing an important role in brain function, adult mice, upon inactivation of *Xrcc1* in the nervous system using a Nes-cre system, exhibit widespread loss of cerebellar interneurons and abnormal activity in hippocampal neurons, resulting in pronounced neurological dysfunction characterized by progressive mild ataxia accompanied by episodic spasms (16).

In addition to determining the consequences of haploinsufficiency of XRCC1 in the absence of exposure, we evaluated the susceptibility of *Xrcc1*$^{+/-}$ mice to AOM, since many environmental agents have the capacity to generate DNA lesions that require XRCC1 for efficient repair. Consistent with evidence that reduced XRCC1 function may be related to disease susceptibility, namely cancer risk (24), we found that (i) *Xrcc1*$^{+/-}$ bone marrow cells were hypersensitive to treatments with the alkylator MMS and (ii) HZ mice exposed to AOM had an increase in aberrant crypt foci in the colon, which are generally accepted as precancerous lesions. The fact that we saw an occasional adenomatous polyp in HZ but not WT mice may be indicative of increased colon tumors in HZ mice had we monitored the animals for a longer period of time. In addition, the rather robust susceptibility of HZ mice treated with AOM to hepatic lesions further emphasizes that XRCC1 plays an important role in attenuating alkylating agent-induced cellular toxicity. The liver has a high propensity for responding to cellular stress, and it was obvious that the early liver necrosis in *Xrcc1*$^{+/-}$ mice, although not life threatening, was progressing toward a chronic inflammatory condition resembling cirrhosis. These observations point to haploinsufficiency in XRCC1, and a defect in SSB repair, being a risk factor in exposure-dependent disease, as well as a need for further evaluation of the effects of exogenous challenges on risk of *Xrcc1* HZ mice, with an eye towards cancer development and neurological dysfunction.

XRCC1 has been reported to be exclusively nuclear, with no mitochondrial localization (8). This restricted intracellular distribution may in part be why no obesity was seen in the *Xrcc1*$^{+/-}$ mice, as the connection between NEIL1 deficiency and pathologies that resemble hypermetabolic syndrome has been argued to stem from a defect in mitochondrial DNA repair (26). Thus, given that mitochondrial DNA repair is presumably normal in *Xrcc1*$^{+/-}$ cells, our results imply that the apparent endodermal-derived developmental malformations, possible stroke propensity and exposure-dependent susceptibility are explicitly related to nuclear genome dynamics.

It remains to be determined if sporadic loss of heterozygosity of XRCC1 in mammals would give rise to more profound consequences on genome integrity and overall organ fitness. Interestingly, a previous report found that an ~10% XRCC1 protein level is sufficient to permit mouse embryogenesis and post-natal development, and that fibroblasts derived from these transgenic mice exhibit little or no increased sensitivity to MMS as determined by a non-quantitative differential cytotoxicity assay (36). Further evaluation of these hypomorph animals revealed that they are consistently smaller than their littermates (~25% reduction in body weight), suggesting an effect of XRCC1 deficiency that is not presently understood (17). Looking forward, it would be of interest to investigate the phenotype of the XRCC1 hypomorph animals in greater detail, both with and without exposure, as well as how specific alterations in XRCC1 function would affect gross pathological outcomes using additional mouse models. For example, two mouse lines have been generated that express a strategic point mutation in either the N-terminal or BRCT1 domain of XRCC1 that disrupts the interaction with POLβ or PARP1, respectively [(17) and unpublished data]. Using these models, it will be possible to determine the precise role of the different XRCC1 molecular functions to any associated disease development.

SUPPLEMENTARY DATA

Supplementary Data are available at NAR Online.

ACKNOWLEDGEMENTS

The authors thank Ms Donna Tignor, Ms Heather Breighner, Dr Jeff Bell, Dr Suresh Poosala, Dr Sylvia Singletary, James Hopkins, Tina Smith and Lisa Burheimer for their support in various capacities with the lifespan studies; Dr Shengyuan Luo and his group for the genotyping efforts; Ms Julissa Villarreal for assistance with coordinating behavioral studies; Dr Susan Tarry (University of Texas Medical Branch, Galveston, TX) for medical input; and Dr Pat Gearhart and Dr Huseyin Saribasak for sharing their unpublished observations.

FUNDING

Funding for open access charge: Intramural Research Program of the National Institute on Aging and National Institute of Environmental Health Sciences grant R21ES016572 (to W.L.).

Conflict of interest statement. None declared.

REFERENCES

1. Lindahl,T. (1993) Instability and decay of the primary structure of DNA. *Nature*, **362**, 709–715.
2. Hoeijmakers,J.H. (2001) Genome maintenance mechanisms for preventing cancer. *Nature*, **411**, 366–374.
3. Kulkarni,A. and Wilson,D.M. III (2008) The involvement of DNA-damage and -repair defects in neurological dysfunction. *Am. J. Hum. Genet.*, **82**, 539–566.
4. Wilson,D.M. III, Bohr,V.A. and McKinnon,P.J. (2008) DNA damage, DNA repair, ageing and age-related disease. *Mech. Ageing Dev.*, **129**, 349–352.
5. Wilson,D.M. III and Bohr,V.A. (2007) The mechanics of base excision repair, and its relationship to aging and disease. *DNA Repair*, **6**, 544–559.
6. Tomkinson,A.E., Vijayakumar,S., Pascal,J.M. and Ellenberger,T. (2006) DNA ligases: structure, reaction mechanism, and function. *Chem. Rev.*, **106**, 687–699.
7. Caldecott,K.W. (2003) XRCC1 and DNA strand break repair. *DNA Repair*, **2**, 955–969.
8. Lakshmipathy,U. and Campbell,C. (2000) Mitochondrial DNA ligase III function is independent of Xrcc1. *Nucleic Acids Res.*, **28**, 3880–3886.
9. Wilson,D.M. III (2007) Processing of nonconventional DNA strand break ends. *Environ. Mol. Mutagen.*, **48**, 772–782.
10. Caldecott,K.W. (2008) Single-strand break repair and genetic disease. *Nat. Rev. Genet.*, **9**, 619–631.
11. Shen,J., Gilmore,E.C., Marshall,C.A., Haddadin,M., Reynolds,J.J., Eyaid,W., Bodell,A., Barry,B., Gleason,D., Allen,K.

et al. (2010) Mutations in PNKP cause microcephaly, seizures and defects in DNA repair. *Nat. Genet*., **42**, 245–249.
12. Takashima,H., Boerkoel,C.F., John,J., Saifi,G.M., Salih,M.A., Armstrong,D., Mao,Y., Quiocho,F.A., Roa,B.B., Nakagawa,M. *et al*. (2002) Mutation of TDP1, encoding a topoisomerase I-dependent DNA damage repair enzyme, in spinocerebellar ataxia with axonal neuropathy. *Nat. Genet*., **32**, 267–272.
13. Date,H., Onodera,O., Tanaka,H., Iwabuchi,K., Uekawa,K., Igarashi,S., Koike,R., Hiroi,T., Yuasa,T., Awaya,Y. *et al*. (2001) Early-onset ataxia with ocular motor apraxia and hypoalbuminemia is caused by mutations in a new HIT superfamily gene. *Nat. Genet*., **29**, 184–188.
14. Moreira,M.C., Barbot,C., Tachi,N., Kozuka,N., Uchida,E., Gibson,T., Mendonca,P., Costa,M., Barros,J., Yanagisawa,T. *et al*. (2001) The gene mutated in ataxia-ocular apraxia 1 encodes the new HIT/Zn-finger protein aprataxin. *Nat. Genet*., **29**, 189–193.
15. Kulkarni,A., McNeill,D.R., Gleichmann,M., Mattson,M.P. and Wilson,D.M. III (2008) XRCC1 protects against the lethality of induced oxidative DNA damage in nondividing neural cells. *Nucleic Acids Res*., **36**, 5111–5121.
16. Lee,Y., Katyal,S., Li,Y., El-Khamisy,S.F., Russell,H.R., Caldecott,K.W. and McKinnon,P.J. (2009) The genesis of cerebellar interneurons and the prevention of neural DNA damage require XRCC1. *Nat. Neurosci*., **12**, 973–980.
17. Ladiges,W.C. (2006) Mouse models of XRCC1 DNA repair polymorphisms and cancer. *Oncogene*, **25**, 1612–1619.
18. Thompson,L.H. and West,M.G. (2000) XRCC1 keeps DNA from getting stranded. *Mutat. Res*., **459**, 1–18.
19. Wilson,D.M. III and Thompson,L.H. (2007) Molecular mechanisms of sister-chromatid exchange. *Mutat. Res*., **616**, 11–23.
20. Tebbs,R.S., Flannery,M.L., Meneses,J.J., Hartmann,A., Tucker,J.D., Thompson,L.H., Cleaver,J.E. and Pedersen,R.A. (1999) Requirement for the Xrcc1 DNA base excision repair gene during early mouse development. *Dev. Biol*., **208**, 513–529.
21. Tkac,I., Starcuk,Z., Choi,I.Y. and Gruetter,R. (1999) In vivo H-1 NMR spectroscopy of rat brain at 1 ms echo time. *Magn. Res. Med*., **41**, 649–656.
22. Rasband,W.S. and Image,J. U. S. National Institutes of Health, Bethesda, Maryland, USA, http://imagej.nih.gov/ij/ (1997–2011).
23. Zijlmans,J.M., Martens,U.M., Poon,S.S., Raap,A.K., Tanke,H.J., Ward,R.K. and Lansdorp,P.M. (1997) Telomeres in the mouse have large inter-chromosomal variations in the number of T2AG3 repeats. *Proc. Natl Acad. Sci. USA*, **94**, 7423–7428.
24. Jiang,J., Zhang,X., Yang,H. and Wang,W. (2009) Polymorphisms of DNA repair genes: ADPRT, XRCC1, and XPD and cancer risk in genetic epidemiology. *Methods Mol. Biol*., **471**, 305–333.
25. Berquist,B.R., Singh,D.K., Fan,J., Kim,D., Gillenwater,E., Kulkarni,A., Bohr,V.A., Ackerman,E.J., Tomkinson,A.E. and Wilson,D.M. III (2010) Functional capacity of XRCC1 protein variants identified in DNA repair-deficient Chinese hamster ovary cell lines and the human population. *Nucleic Acids Res*., **38**, 5023–5035.
26. Vartanian,V., Lowell,B., Minko,I.G., Wood,T.G., Ceci,J.D., George,S., Ballinger,S.W., Corless,C.L., McCullough,A.K. and Lloyd,R.S. (2006) The metabolic syndrome resulting from a knockout of the NEIL1 DNA glycosylase. *Proc. Natl Acad. Sci. USA*, **103**, 1864–1869.
27. Enns,L.C., Morton,J.F., Mangalindan,R.S., McKnight,G.S., Schwartz,M.W., Kaeberlein,M.R., Kennedy,B.K., Rabinovitch,P.S. and Ladiges,W.C. (2009) Attenuation of age-related metabolic dysfunction in mice with a targeted disruption of the Cbeta subunit of protein kinase A. *J. Gerontol. A Biol. Sci. Med. Sci*., **64**, 1221–1231.
28. Chen,J. and Huang,X.F. (2009) The signal pathways in azoxymethane-induced colon cancer and preventive implications. *Cancer Biol. Ther*., **8**, 1313–1317.
29. Wilson,D.M. III, Kim,D., Berquist,B.R. and Sigurdson,A.J. (2010) *Variation* in base excision repair capacity. *Mutat. Res*., [Epub ahead of print].
30. Wilson,D.M. III and Thompson,L.H. (1997) Life without DNA repair. *Proc. Natl Acad. Sci. USA*, **94**, 12754–12757.
31. McKinnon,P.J. (2009) DNA repair deficiency and neurological disease. *Nat. Rev. Neurosci*., **10**, 100–112.
32. Fujimura,M., Morita-Fujimura,Y., Sugawara,T. and Chan,P.H. (1999) Early decrease of XRCC1, a DNA base excision repair protein, may contribute to DNA fragmentation after transient focal cerebral ischemia in mice. *Stroke*, **30**, 2456–2462.
33. Li,N., Wu,H., Yang,S. and Chen,D. (2007) Ischemic preconditioning induces XRCC1, DNA polymerase-beta, and DNA ligase III and correlates with enhanced base excision repair. *DNA Repair*, **6**, 1297–1306.
34. Dutra,A.V., Lin,H.F., Juo,S.H., Mohrenweiser,H., Sen,S. and Grewal,R.P. (2006) Analysis of the XRCC1 gene as a modifier of the cerebral response in ischemic stroke. *BMC Med. Genet*., **7**, 78.
35. Mahabir,S., Abnet,C.C., Qiao,Y.L., Ratnasinghe,L.D., Dawsey,S.M., Dong,Z.W., Taylor,P.R. and Mark,S.D. (2007) A prospective study of polymorphisms of DNA repair genes XRCC1, XPD23 and APE/ref-1 and risk of stroke in Linxian, China. *J. Epidemiol. Community Health*, **61**, 737–741.
36. Tebbs,R.S., Thompson,L.H. and Cleaver,J.E. (2003) Rescue of Xrcc1 knockout mouse embryo lethality by transgene-complementation. *DNA Repair*, **2**, 1405–1417.